Systematic investigation on the validity of partition model dosimetry for ^{90}Y radioembolization using Monte Carlo simulation

2017 Phys. Med. Biol. 62 7342

(http://iopscience.iop.org/0031-9155/62/18/7342)

IOP Publishing | Institute of Physics and Engineering in Medicine Physics in Medicine & Biology

Phys. Med. Biol. **62** (2017) 7342–7356 https://doi.org/10.1088/1361-6560/aa7e5b

Systematic investigation on the validity of partition model dosimetry for ^{90}Y radioembolization using Monte Carlo simulation

Nurul Ab Aziz Hashikin[1,2], Chai-Hong Yeong[1,2], Susanna Guatelli[3], Basri Johan Jeet Abdullah[1], Kwan-Hoong Ng[1,2], Alessandra Malaroda[3], Anatoly Rosenfeld[3] and Alan Christopher Perkins[4]

[1] Department of Biomedical Imaging, Faculty of Medicine, University of Malaya, 50603, Kuala Lumpur, Malaysia
[2] University of Malaya Research Imaging Centre, Faculty of Medicine, University of Malaya, 50603, Kuala Lumpur, Malaysia
[3] Centre for Medical Radiation Physics, Faculty of Engineering and Information Sciences, University of Wollongong, Wollongong, New South Wales, 2522, Australia
[4] Radiological and Imaging Sciences, Medical Physics and Clinical Engineering, Medical School, University of Nottingham, Nottingham, NG7 2UH, United Kingdom

E-mail: chyeong@um.edu.my

Received 7 March 2016, revised 3 July 2017
Accepted for publication 7 July 2017
Published 22 August 2017

Abstract

We aimed to investigate the validity of the partition model (PM) in estimating the absorbed doses to liver tumour (D_T), normal liver tissue (D_{NL}) and lungs (D_L), when cross-fire irradiations between these compartments are being considered. MIRD-5 phantom incorporated with various treatment parameters, i.e. tumour involvement (TI), tumour-to-normal liver uptake ratio (T/N) and lung shunting (LS), were simulated using the Geant4 Monte Carlo (MC) toolkit. 10^8 track histories were generated for each combination of the three parameters to obtain the absorbed dose per activity uptake in each compartment ($D_T^{A_T}$, $D_{NL}^{A_{NL}}$, and $D_L^{A_L}$). The administered activities, A were estimated using PM, so as to achieve either limiting doses to normal liver, D_{NL}^{lim} or lungs, D_L^{lim} (70 or 30 Gy, respectively). Using these administered activities, the activity uptake in each compartment (A_T, A_{NL}, and A_L) was estimated and multiplied with the absorbed dose per activity uptake attained using the MC simulations, to obtain the actual dose received by each compartment. PM overestimated D_L by 11.7% in all cases, due to the escaped particles from the lungs. D_T and D_{NL} by MC were largely affected by T/N, which were not considered by

PM due to cross-fire exclusion at the tumour-normal liver boundary. These have resulted in the overestimation of D_T by up to 8% and underestimation of D_{NL} by as high as −78%, by PM. When D_{NL}^{lim} was estimated via PM, the MC simulations showed significantly higher D_{NL} for cases with higher T/N, and LS ⩽ 10%. All D_L and D_T by MC were overestimated by PM, thus D_L^{lim} were never exceeded. PM leads to inaccurate dose estimations due to the exclusion of cross-fire irradiation, i.e. between the tumour and normal liver tissue. Caution should be taken for cases with higher TI and T/N, and lower LS, as they contribute to major underestimation of D_{NL}. For D_L, a different correction factor for dose calculation may be used for improved accuracy.

Keywords: Geant4 Monte Carlo, hepatocellular carcinoma, liver tumour, radioembolization, partition model, Yttrium-90

(Some figures may appear in colour only in the online journal)

List of abbreviations

2DT	Two spherical tumours of different sizes
2ET	Two spherical tumours of equal size
4ET	Four spherical tumours of equal size
A_T	Activity uptake in tumour
A_{NL}	Activity uptake in normal liver
A_L	Activity uptake in lungs
CPE	Charged particle equilibrium
D_L	Absorbed dose to lungs
$D_L^{A_L}$	Lungs absorbed dose per activity uptake in lungs
D_L^{lim}	Limiting absorbed dose to lungs
D_{NL}	Absorbed dose to normal liver
$D_{NL}^{A_{NL}}$	Normal liver absorbed dose per activity uptake in normal liver
D_{NL}^{lim}	Limiting absorbed dose to normal liver
D_T	Absorbed dose to tumour
$D_T^{A_T}$	Tumour absorbed dose per activity uptake in tumour
HCC	Hepatocellular carcinoma
LS	Lung shunting
MAA	Macro-aggregated albumin
MC	Monte Carlo
MIRD	Medical Internal Radiation Dose
PM	The partition model
S/V	Surface area-to-volume ratio
TI	Tumour involvement
T/N	Tumour-to-normal liver uptake ratio

1. Introduction

Hepatic cancer is the second most common cause of death from cancer worldwide (Ferlay *et al* 2015). The most common type of hepatic cancer is hepatocellular carcinoma (HCC), which is derived from the main cell of the liver called hepatocyte. Transarterial radioembolization

using Yttrium-90 (^{90}Y) microspheres has been increasingly used in the treatment of primary and secondary hepatic malignancies. ^{90}Y decays via beta emissions (mean and maximum energies of 0.93 and 2.28 MeV, respectively) with physical half-life of 64.1 h (ICRP 2008). The current commercially available ^{90}Y microspheres are the resin-based SIR-Spheres® (SIRTEX, Australia) and the glass-based TheraSphere® (Nordion, Canada). These microspheres differ in terms of specific activity (50 versus 2500 Bq per microsphere, respectively) and total number of injected microspheres (60 million versus 1.2–8 million, respectively). Hence, they are available in fixed activity of 3 GBq for SIR-Spheres® (SIRTEX 2004), and six different activity sizes of 3, 5, 7, 10, 15, and 20 GBq for TheraSphere® (Nordion 2004).

^{90}Y radioembolization is commonly performed on patients in the intermediate to advanced stages of the disease, where surgical resection is no longer an option. The treatment is typically delivered to achieve a tumour-absorbed dose, D_T of 100–120 Gy (Salem *et al* 2006, Kennedy *et al* 2007, Dezarn *et al* 2011, Garin *et al* 2015b), which creates a balance between safety and effectiveness (Salem *et al* 2006, Kennedy *et al* 2007). In order to minimise the risk of radiation pneumonitis, extrahepatic shunting of the microspheres especially to the lungs is assessed, prior to the treatment, using Technetium-99m (^{99m}Tc) macro-aggregated albumin (MAA) (SIRTEX 2015). The lung shunting (LS); that is the percentage of activity taken up by the lungs with respect to the administered activity, should be lower than 20%, to limit the absorbed dose to the lungs, D_L from exceeding the limiting dose, D_L^{lim} of 30 Gy per treatment session, and 50 Gy cumulatively (Ho *et al* 1997, Garin *et al* 2015b). Moreover, a limiting normal liver dose, D_{NL}^{lim} of 70 Gy is recommended, in order to avoid severe impairment of the liver function following the treatment (Lau *et al* 2012, SIRTEX 2015).

In estimating these doses, the most widely used dosimetric approach is the partition model (PM), which assumes a local energy deposition with no consideration of cross-fire between the liver tumour and normal liver tissue (Ho *et al* 1996, Garin *et al* 2015b, SIRTEX 2015). This assumption, however, is inaccurate as tumour vascularity has the tendency to be distributed at the periphery of the tumour (Fox *et al* 1991, Campbell *et al* 2000, 2001, Kennedy *et al* 2004). Thus, most of the ^{90}Y microspheres will be deposited at the tumour boundary rather than uniformly distributed within the tumour. Since ^{90}Y beta particles have a relatively long range in tissue (maximum of about 1 cm), some particles originated from the tumour will deposit energy in the normal liver tissue. In this context, the increased vascularity of the tumour surface would heighten the cross-fire irradiation.

The absorbed doses estimated using PM have been previously compared with the doses measured using an intraoperative beta probing (Ho *et al* 1996). Although correlations were found between the measured and calculated data, the discrepancies were still large with mean dose differences of 14.8 ± 14.0 and 15.1 ± 27.2% for tumour and normal liver, respectively. Also, the highly invasive approach is considered impractical and contradictive to radioembolization, which is minimally invasive. Personalised dosimetry has been demonstrated in previous studies for improved lung dosimetry (Kao *et al* 2014), as well as to investigate the response rate and survival (Garin *et al* 2015a) of the HCC patients, however, both methods were still largely dependent on the PM equations. Several publications have recommended the use of Monte Carlo (MC) simulations in estimating the absorbed doses in radioembolization (Kennedy *et al* 2004, Sarfaraz *et al* 2004, Flamen *et al* 2008, Gulec *et al* 2010, Kao *et al* 2011, Garin *et al* 2015b). It is expected that the MC method is more accurate in estimating the doses delivered to the tumour and surrounding healthy tissues compared to PM, because the energy deposition in a medium is calculated without adopting any simplified assumption in terms of particle transportation. Geant4 (Agostinelli *et al* 2003, Allison *et al* 2006, 2016) has been increasingly used for the estimation of absorbed doses in nuclear medicine, with its

accuracy validated through experimental measurements using physical phantoms (Meo *et al* 2008, Ziaur *et al* 2012).

The aim of this study was to investigate the accuracy of the absorbed doses estimated by PM, as a result of the exclusion of cross-fire irradiation, especially between the tumour and normal liver tissue. Geant4 MC simulations were carried out and the resulting absorbed doses were compared with the doses calculated using PM. The factors that may affect the accuracy of PM estimations were determined and discussed in this study.

2. Methods

2.1. The PM

PM estimates the absorbed dose to tumour (D_T), normal liver tissue (D_{NL}), and lungs (D_L). It was derived by Ho *et al* (1996) and it assumes that the radioactive microspheres are distributed only in the three compartments, with no redistribution during the treatment. The model was derived from the decay data of ^{90}Y and, assuming a complete deposition of energy within a compartment, it depends only on the initial activity in the compartment and the compartment's total mass (Ho *et al* 1996). Thus, the absorbed dose, D (Gy) in a compartment of mass, M (kg), containing an initial ^{90}Y activity, A_o (GBq) is expressed as in equation (1) (Ho *et al* 1996):

$$D = \frac{49.67 A_o}{M} \tag{1}$$

where, 49.67 Gy · kg · GBq^{-1} is the emitted energy (J) per ^{90}Y nuclear transformation (decay) per mass (kg).

In order to determine the activity distributed within each organ, the LS and tumour-to-normal liver uptake ratio (T/N) are obtained from the pre-treatment imaging using ^{99m}Tc-MAA (Lau *et al* 1994, Leung *et al* 1994). For patients to be considered eligible for the treatment with ^{90}Y microspheres, the LS should not be larger than 20%. For patients with LS of between 10% to 15% and 15% to 20%, the administered activities need to be reduced by 20% and 40%, respectively (SIRTEX 2015) to limit the D_L from exceeding 30 Gy. Therefore, the activity uptake in the lungs, A_L is calculated using equation (2) (Ho *et al* 1996), where, A is the administered activity.

$$A_L = A \frac{\mathrm{LS}(\%)}{100} \tag{2}$$

The remaining activity is assumed to be taken up by the tumour, A_T and normal liver tissue, A_{NL} as in equation (3) (Ho *et al* 1996), with the T/N given by equation (4) (Ho *et al* 1996):

$$A_T + A_{NL} = A - A_L \tag{3}$$

$$\mathrm{T/N} = \frac{A_T/M_T}{A_{NL}/M_{NL}} \tag{4}$$

where, M_T and M_{NL} are the masses (kg) of the tumour and normal liver tissue, respectively.

2.2. The Geant4 MC application

This study was carried out using the Geant4 version 9.6.p03 (Agostinelli *et al* 2003, Allison *et al* 2006). As in the Geant4 advanced example *human_phantom*, a mathematical adult human

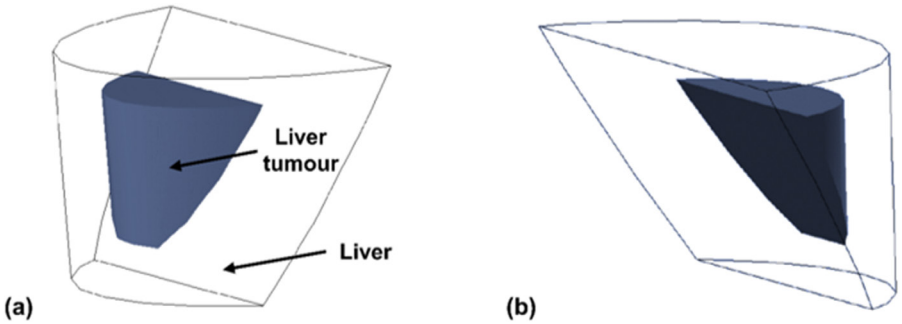

Figure 1. (a) Antero-superior and (b) postero-superior view of the tumour model for 10% TI.

phantom was modelled according to the Medical Internal Radiation Dose (MIRD) Pamphlet 5 consisting of complete anatomical organs (Snyder *et al* 1978). The 70 kg MIRD-5 phantom comprises three types of tissues namely the bone, lung, and soft tissue (densities of 1.4862, 0.2958, and 0.9869 $g \cdot cm^{-3}$, respectively). The mass of each lung (right and left) and liver are 0.5 and 1.809 kg, respectively.

2.2.1. Computational phantom. In this study, a single tumour with similar shape to the mathematical MIRD-5 liver, located at the centre of the liver and varying in mass, was considered (figure 1). The tumour mass, M_T is defined by the tumour involvement (TI) (%), as calculated using equation (5):

$$M_T = 0.01\,TI\,M_L \tag{5}$$

where, M_L is the mass of the liver. Additional simulations with single and multiple spherical tumours, each corresponding to 10% TI were also carried out for comparison. These include simulations of (i) a single tumour; (ii) two tumours of equal size (2ET) with 5% TI each; (iii) two tumours of different sizes (2DT) with 3% and 7% TI, respectively; and (iv) four tumours of equal size (4ET) with 2.5% TI each. These tumours were placed with sufficient separation that the cross-fire between them was less than 1% of the D_T. This was first validated during the construction of the application, prior to the actual simulations. The surface area-to-volume ratios (S/V) for the tumours are shown in table 1. The liver surface area, as estimated by the MC methods is 1724.0 cm^2; i.e. liver S/V is 0.94 cm^{-1}.

2.2.2. Details on the Geant4 simulation. The Low Energy Electromagnetic package (Chauvie *et al* 2004) was adopted to model the electromagnetic interactions, providing more accurate physics modelling at low energies with respect to the Geant4 standard package. This package provides the description of physics processes for photons, electrons, charged hadrons, and ions, down to 250 eV. The threshold of production of secondary particles was fixed to 1 mm.

The Geant4 Radioactive Decay component which consisted of radionuclide decay data based on the Evaluated Nuclear Structure Data File (Tuli 1987), was used to model the decay spectrum of ^{90}Y. The Geant4 General Particle Source was used to model the radionuclide in the tumour. ^{90}Y point sources were homogenously distributed within each compartment with activity uptake based on the selected T/N and LS, with randomised direction of emissions. The tumour, normal liver, and right and left lung were each set as a sensitive volume. The output was set as the mean energy (MeV) deposited to each volume.

Table 1. S/Vs (cm^{-1}) for the tumour models of this work.

TI (%)	Tumour model	Mass (g)	Surface area (cm^2)	Volume (cm^3)	S/V (cm^{-1})
10	Single sphere	180.9	156.1	183.3	0.85
10	Two spheres; equal size (2ET)	180.9	196.6	183.3	1.07
10	Two spheres; different sizes (2DT)	180.9	193.0	183.3	1.05
10	Four spheres; equal size (4ET)	180.9	247.8	183.3	1.35
10	Single non-spherical	180.9	577.8	183.3	3.15
30	Single non-spherical	542.7	944.5	549.9	1.72
50	Single non-spherical	904.5	1222.6	916.5	1.33
70	Single non-spherical	1266.3	1426.9	1283.1	1.11

2.3. Effects of various patient parameters on the absorbed dose

The effects of various TI (10%, 30%, 50%, 70%), T/N (1, 2.5, 5, 7.5, 10), and LS (0%, 5%, 10%, 15%, 20%; without the reduction in the administered activity for cases where LS $>$ 10% as recommended by SIRTEX (2015)) on the accuracy of the absorbed doses estimated by PM were investigated. The minimum and maximum values for TI and T/N were decided based on the clinical cases used in the Ho *et al* (1996) study, where the range of TI and T/N were 12%–65% (mean: 39%) and 3–14 (but only 1/17 cases with T/N $>$ 10; mean: 6), respectively. In addition, Goin *et al* (2005) mentioned that the ideal candidates for ^{90}Y radioembolization are those who do not have infiltrative HCC or bulk disease ($\geqslant$70% tumour replacement of liver). On the other hand, patients with very small tumours are not candidates for this treatment (Han *et al* 2011). For LS, the maximum value was chosen based on the maximum LS allowed for treatment (20%) (SIRTEX 2015). The intervals were randomly decided according to practicality in terms of simulation time.

10^8 disintegrations (corresponded to 300 Bq of ^{90}Y) were generated for each simulation and repeated three times with different random seeds, to obtain a standard deviation of less than 1%. The mean energy (MeV) deposited within each compartment per simulated ^{90}Y decay was expressed in joules (J) and divided by the mass of the compartment (kg), to obtain the absorbed dose (Gy). The results were expressed as the absorbed dose per activity uptake ($mGy \cdot MBq^{-1}$), by dividing each estimated dose with the activity taken up by the corresponding compartment.

Using PM, the administered activities for treatments with different parameter combinations were estimated, so as to achieve either D_{NL}^{lim} or D_{L}^{lim} of 70 or 30 Gy, respectively. From these administered activities, the activity uptake in each compartment was estimated using equation (3). These activities were then multiplied with the absorbed dose per activity uptake values as calculated from the simulations, to obtain the actual absorbed doses received by each compartment. The absorbed doses obtained from the two methods (PM versus MC) were compared, and the parameter combinations contributing to differences in the estimated D_L and D_{NL} were identified.

3. Results

3.1. Comparison of absorbed dose estimates (PM versus MC)

The absorbed dose per activity uptake in tumour, $D_T^{A_T}$ and normal liver, $D_{NL}^{A_{NL}}$ with various TI and T/N are shown in tables 2 and 3, respectively. LS does not affect both $D_T^{A_T}$ and $D_{NL}^{A_{NL}}$. The $D_T^{A_T}$ and $D_{NL}^{A_{NL}}$ by PM are not affected by the T/N. Rather, they only depend on the TI.

Table 2. Tumour absorbed dose per activity uptake in tumour, $D_T^{A_T}$ calculated by PM and MC simulation.

	Absorbed dose per activity uptake in tumour (mGy · MBq^{-1})					
		MC simulation				
		T/N				
TI (%)	PM (all T/N)	1	2.5	5	7.5	10
10	274.57	275.13	259.97	254.92	253.28	252.41
30	91.52	91.70	88.45	87.37	87.00	86.82
50	54.91	55.02	53.40	52.87	52.69	52.60
70	39.22	39.27	38.27	37.93	37.82	37.76

Table 3. Normal liver tissue absorbed dose per activity uptake in normal liver tissue, $D_{NL}^{A_{NL}}$ calculated by PM and MC simulation.

	Absorbed dose per activity uptake in normal liver (mGy · MBq^{-1})					
		MC simulation				
		T/N				
TI (%)	PM (all T/N)	1	2.5	5	7.5	10
10	30.51	29.28	29.75	30.53	31.31	32.09
30	39.22	37.18	38.67	41.17	43.66	46.15
50	54.91	50.87	54.92	61.65	68.37	75.10
70	91.52	80.27	94.00	116.92	139.75	162.71

However, as can be seen in the tables, our simulations show that T/N indeed affects both $D_T^{A_T}$ and $D_{NL}^{A_{NL}}$. The $D_L^{A_L}$ (for all T/N and LS; except for LS of 0%) generated by PM and MC were 49.67 ± 0.00 and 43.84 ± 0.01 mGy · MBq^{-1}, respectively. This corresponds to a relative difference of 11.74 ± 0.03% between the two methods, with respect to PM.

Figures 2 and 3 show the relative differences between the absorbed doses estimated by the two methods (for tumour and normal liver, respectively) for various TI and T/N, with respect to PM. For tumour, the relative differences are observed to be larger for lower TI and higher T/N, with maximum dose overestimation of up to 8% by PM.

For normal liver, the relative differences for T/N of less than 2 were larger for higher TI and lower T/N by up to 12.3%. However, as T/N goes beyond 2, the relative differences drastically shift to negative values with larger differences observed for higher TI and T/N, up to a maximum difference of −78%. From figure 3, we found that at T/N of approximately 2, the relative differences for all TI are equal with values of about 3%, with respect to PM.

Figure 4 shows the relative differences between the D_T estimated by the two methods (with respect to PM) for various tumour models, where each corresponds to a total TI of 10%. The single-sphere model showed the lowest relative differences compared to the other models. The single non-spherical model showed larger differences of up to 3.1%, relative to its spherical counterpart. As the number of spheres increases, the relative differences also increase, although each model represents similar TI. For equal number of spheres but with variations in the spherical sizes (2ET versus 2DT), the results showed that there were only very minute differences (<0.5%) between the two models, with the 2ET model showing slightly higher relative differences. The 4ET model showed the highest relative differences of up to 8.3%, only slightly higher (<0.2%) than the differences noted for the non-spherical model.

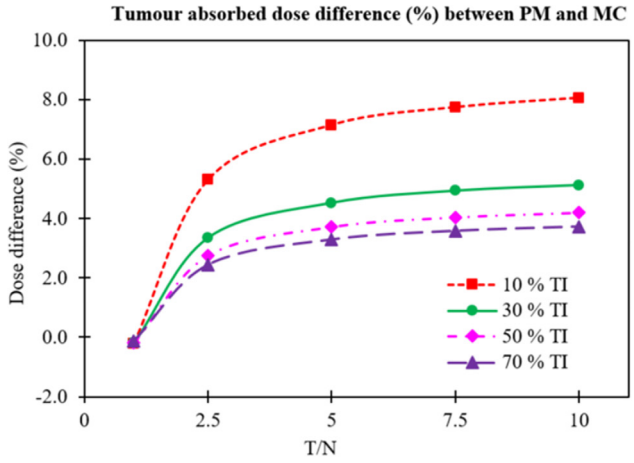

Figure 2. Tumour absorbed dose difference (%) between the PM and MC simulations for various TI and T/N, normalised to PM.

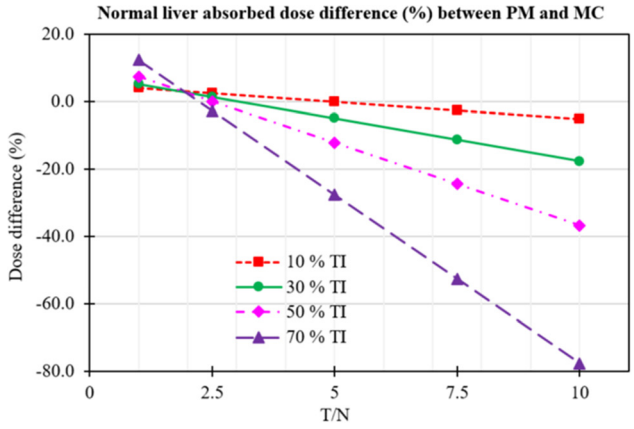

Figure 3. Normal liver absorbed dose difference (%) between the PM and MC simulations for various TI and T/N, normalised to PM.

3.2. Implications of the absorbed dose in treatment planning

Amongst 100 simulated cases, 28 cases where the D_{NL} estimated by MC exceeded the D_{NL}^{lim} were determined and are listed in table 4. Since PM overestimated D_L by 11.7%, the MC-derived D_L never exceeds D_L^{lim}. All cases in table 4 involved LS values equal to or lower than 10%, with most T/N equal to or larger than 5 (only two cases with T/N of 2.5). The mean administered activity was 8.51 $\pm$ 3.65 GBq, with minimum and maximum activity of 4.21 and 18.61 GBq, respectively. D_T as estimated by PM were in the range of 175–700 Gy, but MC estimated a significantly lower range of D_T. Out of the 28 cases, only four (cases no. 13, 19, 26, and 27) were estimated by PM to reach D_L^{lim} (hence, D_{NL} should be lower than D_{NL}^{lim}), but D_{NL}^{lim} were still exceeded. Two cases (cases no. 22 and 23) with D_{NL} of larger than 100 Gy were recorded by the liver with 70% TI.

Table 5 compares the PM- and MC-based estimates of the administered activity for the cases of table 4, where the MC simulations limited D_{NL} to 70 Gy. Administered activity differences of up to 44% were observed (case no. 23) with a mean difference of 12.2% $\pm$ 10.6%.

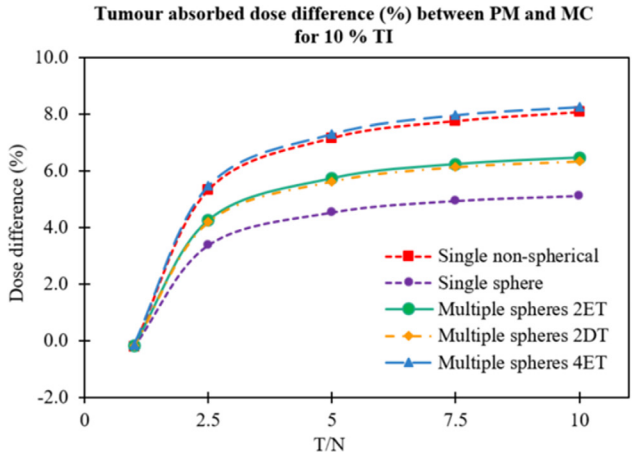

Figure 4. Tumour absorbed dose difference (%) between the PM and MC simulations for 10% TI with various tumour models and T/N, normalised to PM. 2ET: two tumours with equal size; 2DT: two tumours with different sizes; 4ET: four tumours with equal size.

4. Discussion

PM was derived by Ho *et al* (1996) from the decay data of ^{90}Y, where 0.037 MBq taken up by 1 g of tissue will result in an absorbed dose of 183.78 cGy. Following simplification, this has resulted in the constant value of 49.67 Gy · kg · GBq^{-1}, which is used in the main formula (equation (1)) for the absorbed dose estimation (Ho *et al* 1996). Our MC simulations successfully demonstrated the cross-fire phenomenon, which has been neglected by PM, with PM constantly overestimating the D_{L} by 11.7%. This was caused by the escaped particles near the lung boundary and even from deep in the lungs (since beta has longer range in lower-density material). Using this finding, equation (1) can be corrected exclusively for the estimation of D_{L}, by multiplying 0.883 with 49.67, as shown in equation (6).

$$D_{\mathrm{L}} = \frac{43.86\,A_{\mathrm{L}}}{M_{\mathrm{L}}} \tag{6}$$

where, M_{L} is the mass of the lungs. However, it should be noted that the suggested coefficient is dependent on the assumed mathematical modelling of the MIRD-5 phantom. From our study, we did not find any significant contribution of D_{L} from the radiation in the liver as a result of the phantom geometry used in the study, where the liver and lungs separation distance is larger than the maximum beta range of ^{90}Y (11 mm).

As mentioned in section 2.2.1, the single-spherical-tumour model was limited to a maximum of 18% TI, hence, the model was not used in our study. Consequently, the attempts to incorporate multiple spherical tumours into the liver to represent TI larger than 10% have been carried out (up to TI of nearly 30%). However, the efforts were restricted, since extensive geometrical construction time was required in order to arrange all the spheres without interceptions between them. Also, in order to fit all the spheres into the liver, various number of spheres and spherical sizes can be used to represent the desired TI, which will lead to variations in the results. This is because the decisions on how many spheres and which spherical sizes to be used are rather arbitrary. For simplicity, additional simulations to compare different tumour models have been carried out for 10% TI, to investigate the effects of the number of

Table 4. Cases where the normal liver absorbed dose, D_{NL} (based on MC simulations) exceeded the maximum limit, D_{NL}^{lim} of 70 Gy.

					Absorbed dose (Gy)					
					PM			MC simulation		
No.	TI (%)	LS (%)	T/N	A (GBq)[a]	D_L	D_T	D_{NL}	D_L	D_T	D_{NL}
1	10	0	7.5	4.21	0.0	525.0	70.0	0.0	484.3	71.8
2	10	0	10	4.84	0.0	700.0	70.0	0.0	643.5	73.6
3	10	5	7.5	4.43	11.0	525.0	70.0	9.7	484.3	71.8
4	10	5	10	5.10	12.7	700.0	70.0	11.2	643.5	73.6
5	10	10	7.5	4.67	23.2	525.0	70.0	20.5	484.3	71.8
6	10	10	10	5.38	26.7	700.0	70.0	23.6	643.5	73.6
7	30	0	5	5.61	0.0	350.0	70.0	0.0	334.1	73.5
8	30	0	7.5	7.52	0.0	525.0	70.0	0.0	499.1	77.9
9	30	0	10	9.43	0.0	700.0	70.0	0.0	664.1	82.4
10	30	5	5	5.90	14.7	350.0	70.0	12.9	334.1	73.5
11	30	5	7.5	7.92	19.7	525.0	70.0	17.4	499.1	77.9
12	30	5	10	9.93	24.7	700.0	70.0	21.8	664.1	82.4
13	30	10	5	6.04	30.0	339.2	67.8	26.5	323.8	71.2
14	50	0	5	7.65	0.0	350.0	70.0	0.0	336.9	78.6
15	50	0	7.5	10.84	0.0	525.0	70.0	0.0	503.7	87.2
16	50	0	10	14.02	0.0	700.0	70.0	0.0	670.5	95.7
17	50	5	5	8.05	20.0	350.0	70.0	17.6	337.0	78.6
18	50	5	7.5	11.41	28.3	525.0	70.0	25.0	503.7	87.2
19	50	5	10	12.08	30.0	572.9	57.3	26.5	548.8	78.3
20	70	0	2.5	5.23	0.0	175.0	70.0	0.0	170.7	71.9
21	70	0	5	9.69	0.0	350.0	70.0	0.0	338.5	89.4
22	70	0	7.5	14.15	0.0	525.0	70.0	0.0	506.2	106.9
23	70	0	10	18.61	0.0	700.0	70.0	0.0	673.9	124.4
24	70	5	2.5	5.50	13.7	175.0	70.0	12.1	170.7	71.9
25	70	5	5	10.20	25.3	350.0	70.0	22.4	338.5	89.4
26	70	5	7.5	12.08	30.0	425.8	56.8	26.5	410.6	86.7
27	70	5	10	12.08	30.0	431.6	43.2	26.5	415.5	76.7
28	70	10	2.5	5.81	28.8	175.0	70.0	25.5	170.7	71.9

[a] The administered activities, A listed in the table were estimated by the PM.

spheres and their sizes towards the estimation of D_T. Although the spherical tumours were purposely located towards the liver centre, the distances between them were set so that the particles that managed to escape from a sphere did not end up being absorbed by the other spheres, as mentioned in section 2.2.1. This is to ensure that the estimation of D_T is not being affected, hence the tumours can also be assumed to be located anywhere within the liver.

Even though the simulations were carried out with the tumour located at the centre of the liver, it should be noted that in real cases the tumours may as well be located at the edge of the liver. For these cases, our data on the D_T may still be useful regardless of the tumour location within the liver. However, the D_{NL}, D_L, and doses to the other extrahepatic tissues may be affected depending on the tumour location. We can say that for D_{NL}, the doses will be lower, since as the tumours are located more towards the liver edges, the particles will be less absorbed by the normal liver, but rather end up at the extrahepatic tissues. For this, the doses to the tissues should be evaluated to prepare for any complications resulting from the organ

Table 5. Administered activity, A (GBq) for the cases of table 4 where MC limited D_{NL} to 70 Gy.

	A (GBq)				A (GBq)		
No.	PM-based	MC-based	% difference	No.	PM-based	MC-based	% difference
1	4.21	4.10	2.61	15	10.84	8.70	19.74
2	4.84	4.61	4.75	16	14.02	10.25	26.89
3	4.43	4.31	2.71	17	8.05	7.17	10.93
4	5.10	4.85	4.90	18	11.41	9.16	19.72
5	4.67	4.55	2.57	19	12.08	10.79	10.68
6	5.38	5.12	4.83	20	5.23	5.09	2.68
7	5.61	5.34	4.81	21	9.69	7.58	21.78
8	7.52	6.76	10.11	22	14.15	9.27	34.49
9	9.43	8.02	14.95	23	18.61	10.47	43.74
10	5.90	5.63	4.58	24	5.50	5.36	2.55
11	7.92	7.11	10.23	25	10.20	7.98	21.76
12	9.93	8.44	15.01	26	12.08	9.76	19.21
13	6.04	5.94	1.66	27	12.08	11.02	8.77
14	7.65	6.81	10.98	28	5.81	5.65	2.75

radiation toxicities. If the tissue involved is of the lung, the administered activity should be adjusted prior to treatment so that the D_L does not exceed 30 Gy.

The single-sphere model showed the lowest relative differences as a result of low S/V (thus, fewer beta particles would escape from the tumour), compared to other models of the same mass. Hence, the estimation of D_T using the model is the closest to that of PM. However, differences are still present, since our MC simulations consider the cross-fire effect, which is not included with PM. For the spherical models, as the S/V increases (due to increase in the number of spheres), a similar trend with the increase in the relative differences was observed. However, this is not the case when the single non-spherical model was compared with the 4ET model. Although the S/V of the 4ET model was more than twice as low as that of the single non-spherical model, the relative differences between them were almost identical ($<0.2\%$). This could be as a result of the tumour shapes. Since the 4ET model consisted of separate small spheres (radius 2.22 cm), the probability of the particles to leave the spheres was higher compared to the particles located within the non-spherical model, which consisted of one bulk volume. Since the D_T differences of the single non-spherical model depict that of the 4ET model, we can say that the usage of the non-spherical model for TIs other than 10% was relevant, to represent the distribution of D_T in ^{90}Y radioembolization of unresectable HCC.

As shown in section 3.1, both D_T and D_{NL} obtained by MC are dependent on the T/N, which was ignored by PM, as a result of the exclusion of cross-fire irradiation between the compartments. For the tumour model used in our study, larger D_T overestimation by PM for lower TI was due to higher tumour S/V. Hence, for these tumours, the probability of the beta particles leaving is higher than being self-absorbed. This phenomenon also applies for the estimation of D_{NL} where higher TI (higher normal liver S/V) results in larger D_{NL} differences between PM and MC.

Larger D_T overestimation for higher T/N was due to the higher total number of beta particles leaving the tumour compared to the lower T/N (figure 5). For lower T/N, the fraction of beta particles leaving the tumour is being compensated by the particles entering the tumour from the normal liver. Thus, the estimated D_T is closer to the corresponding dose estimated

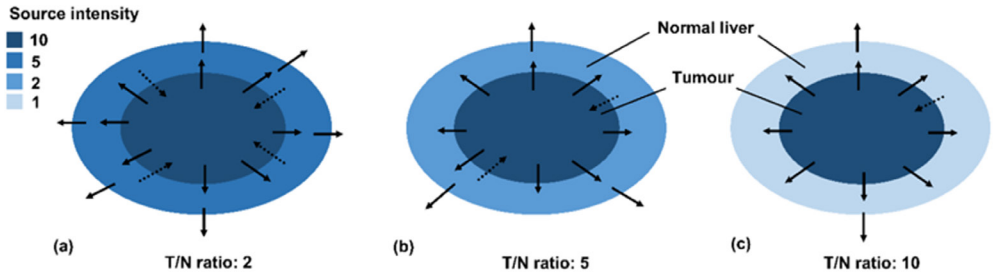

Figure 5. Cross-fire events occurring at the compartment boundaries, which affect the D_T and D_{NL}, as a result of different T/N. (a) Low, (b) medium, and (c) high. D_T: dose to tumour, D_{NL}: dose to normal liver.

by PM. The D_T difference for T/N of 1 was negligible due to charged particle equilibrium (CPE) at the tumour and normal liver boundary. For the estimation of D_{NL}, the transition that occurs at T/N of ~2 can be explained due to CPE. When T/N increases and approaches 2, the particles leaving the normal liver is slowly compensated by the increased number of particles entering from the tumour boundary, as shown in figure 5(a) resulting in D_{NL} overestimation by PM. As the T/N increases beyond 2, the number of particles entering the normal liver from the tumour boundary finally overtakes the total number of particles leaving the normal liver from both tumour and extrahepatic boundaries. Hence, the D_{NL} is higher than estimated by PM, as shown in figures 5(b) and (c).

Even though the maximum difference for D_T between the two methods was only up to 8% and as shown in table 4; where all D_T were being overestimated by PM, this underdosing may lead to less treatment efficiency if we are aiming for a radical approach, especially for smaller tumours. For normal liver, it is a concern for patients with higher TI and T/N, as we found surprisingly high underestimation of D_{NL} up to −78% by PM, which may cause normal liver overdose even when not aiming at D_{NL}^{lim}, as shown in table 4 (case no. 13, 19, 26 and 27). Since it is crucial to reserve the liver function, having a slight increase in the D_{NL} could lead to detrimental effects, especially for larger TI where the reserve normal liver volume is very small. Furthermore, although the administered activities used to achieve either D_{NL}^{lim} or D_L^{lim} were considered to be very high compared to the maximum of 3 GBq recommended for SIR-Spheres® (SIRTEX 2004), they are still highly possible if TheraSphere® is being used. However, we believe this will still be possible for SIR-Spheres® if a whole liver volume of lower than 1.809 kg is being used, which requires less activity to achieve similar doses.

We have demonstrated that PM can be inaccurate in estimating D_T, D_{NL}, and D_L as a result of the exclusion of cross-fire irradiation between the compartments. However, in terms of safety PM is still sufficient in estimating both D_T and D_L, since there is no upper limit to D_T and that D_L^{lim} were never exceeded. Nonetheless, we would recommend that D_L estimation be based on the corrected D_L (equation (6)), for better accuracy. For D_{NL}, caution should be taken in estimating these doses, especially for cases with higher TI and T/N, and lower LS, by possibly administering lower activity (as shown in table 5) or separating the treatment in fractions, in order to promote tissue sparing of the normal liver.

Our study was done using a simple model of the standard MIRD-5 human phantom so as to easily understand the pattern of the physical factors that may affect the absorbed dose estimation, by manipulating the patient parameters accordingly. For wider acceptance, the term 'tumour involvement' can be changed to 'tumour replacement of liver' as used by Goin *et al* (2005) and Lewandowski *et al* (2006). Although the liver model used in this study has a fixed

volume, the findings can be applied to any liver volumes as long as the TI or tumour replacement of the liver correspond to a similar relative value. It should be noted that in real cases, the whole liver volume may be increased as the tumour enlarged, assuming the normal liver volume is not affected. For this case, the TI will be lower (as opposed to the fixed liver model used in our study), even though the tumours in both conditions have a similar mass. Thus, the findings of a lower TI should be used.

Since every patient's tumour is unique (in terms of size, shape, and location), the use of tomographic data may be useful to further estimate the dose to these compartments, with the incorporation of the heterogeneity of both tissue and source distributions, which were not considered in our study. These considerations require additional effort in the preparation of MC code input and simulation time and hence, may not be practical for clinical use. Alternatively, voxel dose kernel (simulating radiation transport in water and applying the dose distribution map into tomographic images) can be used, to reduce the simulation time. However, this method does not take into account the tissue inhomogeneity correction. A recent approach has been found to be able to speed up the simulation time, while at the same time accounting for both tissue and source inhomogeneity (Sanchez-Garcia *et al* 2014), which opens up possibilities of improved dosimetry for ^{90}Y radioembolization of HCC.

5. Conclusion

In conclusion, PM leads to inaccurate dose estimations, due to the exclusion of the cross-fire irradiation, especially between the tumour and normal liver tissue. The inaccuracy is especially concerning for cases with higher TI and T/N, and lower LS, as they contribute to major underestimation of D_{NL}. As for D_L, the suggested coefficient can be implemented exclusively for lungs, for improved accuracy of D_L.

Acknowledgments

A huge appreciation to Mr Wei-Loong Jong from the Department of Oncology, Faculty of Medicine, University of Malaya, Kuala Lumpur, for the guidance and support in carrying out this research.

Funding

This study was funded by the Ministry of Science, Technology and Innovation (MOSTI) Science Fund SF011-2014 and University of Malaya Postgraduate Research Fund PG104-2013B.

Conflict of interest

All authors have declared that they have no conflict of interest.

Ethical approval

This article does not contain any studies by any of the authors involving human participants or animals, and hence no informed consent is needed.

References

Agostinelli S *et al* 2003 Geant4—a simulation toolkit *Nucl. Instrum. Methods* A **506** 250–303

Allison J *et al* 2006 Geant4 developments and applications *IEEE Trans. Nucl. Sci.* **53** 270–8

Allison J *et al* 2016 Recent developments in Geant4 *Nucl. Instrum. Methods* A **835** 186–225

Campbell A M, Bailey I H and Burton M A 2000 Analysis of the distribution of intra-arterial microspheres in human liver following hepatic Yttrium-90 microsphere therapy *Phys. Med. Biol.* **45** 1023–33

Campbell A M, Bailey I H and Burton M A 2001 Tumour dosimetry in human liver following hepatic Yttrium-90 microsphere therapy *Phys. Med. Biol.* **46** 487–98

Chauvie S *et al* 2004 Geant4 low energy electromagnetic physics *IEEE Nuclear Science Symp. Conf. Record (Rome, Italy)* vol 3 pp 1881–5

Dezarn W A *et al* 2011 Recommendations of the American Association of Physicists in Medicine on dosimetry, imaging, and quality assurance procedures for ^{90}Y microsphere brachytherapy in the treatment of hepatic malignancies *Med. Phys.* **38** 4824–45

Ferlay J *et al* 2015 Cancer incidence and mortality worldwide: sources, methods and major patterns in GLOBOCAN 2012 *Int. J. Cancer* **136** E359–86

Flamen P *et al* 2008 Multimodality imaging can predict the metabolic response of unresectable colorectal liver metastases to radioembolization therapy with Yttrium-90 labeled resin microspheres *Phys. Med. Biol.* **53** 6591–603

Fox R A, Klemp P F, Egan G, Mina L L, Burton M A and Gray B N 1991 Dose distribution following selective internal radiation therapy *Int. J. Radiat. Oncol. Biol. Phys.* **21** 463–7

Garin E *et al* 2015a Personalized dosimetry with intensification using ^{90}Y-loaded glass microsphere radioembolization induces prolonged overall survival in hepatocellular carcinoma patients with portal vein thrombosis *J. Nucl. Med.* **56** 339–46

Garin E, Rolland Y, Laffont S and Edeline J 2015b Clinical impact of Tc-MAA SPECT/CT-based dosimetry in the radioembolization of liver malignancies with Y-loaded microspheres *Eur. J. Nucl. Med. Mol. Imaging* **43** 559–75

Goin J E *et al* 2005 Treatment of unresectable hepatocellular carcinoma with intrahepatic Yttrium 90 microspheres: factors associated with liver toxicities *J. Vasc. Interv. Radiol.* **16** 205–13

Gulec S A, Sztejnberg M L, Siegel J A, Jevremovic T and Stabin M 2010 Hepatic structural dosimetry in ^{90}Y microsphere treatment: a Monte Carlo modeling approach based on lobular microanatomy *J. Nucl. Med.* **51** 301–10

Han K H *et al* 2011 Asian consensus workshop report: expert consensus guideline for the management of intermediate and advanced hepatocellular carcinoma in Asia *Oncology* **81** 158–64

Ho S *et al* 1996 Partition model for estimating radiation doses from Yttrium-90 microspheres in treating hepatic tumours *Eur. J. Nucl. Med.* **23** 947–52

Ho S, Lau W Y, Leung T W T, Chan M, Johnson P J and Li A K C 1997 Clinical evaluation of the partition model for estimating radiation doses from Yttrium-90 microspheres in the treatment of hepatic cancer *Eur. J. Nucl. Med.* **24** 293–8

ICRP 2008 Nuclear decay data for dosimetric calculations ICRP Publication 107 *Ann. ICRP* **38** 7–96

Kao Y H *et al* 2014 Personalized predictive lung dosimetry by Technetium-99m macroaggregated albumin SPECT/CT for Yttrium-90 radioembolization *EJNMMI Res.* **4** 33

Kao Y H, Tan E H, Ng C E and Goh S W 2011 Clinical implications of the body surface area method versus partition model dosimetry for Yttrium-90 radioembolization using resin microspheres: a technical review *Ann. Nucl. Med.* **25** 455–61

Kennedy A S *et al* 2007 Recommendations for radioembolization of hepatic malignancies using Yttrium-90 microsphere brachytherapy: a consensus panel report from the radioembolization brachytherapy oncology consortium *Int. J. Radiat. Oncol. Biol. Phys.* **68** 13–23

Kennedy A S, Nutting C, Coldwell D, Gaiser J and Drachenberg C 2004 Pathologic response and microdosimetry of ^{90}Y microspheres in man: review of four explanted whole livers *Int. J. Radiat. Oncol. Biol. Phys.* **60** 1552–63

Lau W Y *et al* 2012 Patient selection and activity planning guide for selective internal radiotherapy with Yttrium-90 resin microspheres *Int. J. Radiat. Oncol. Biol. Phys.* **82** 401–7

Lau W Y *et al* 1994 Diagnostic pharmaco-scintigraphy with hepatic intra-arterial technetium-99m macroaggregated albumin in the determination of tumour to non-tumour uptake ratio in hepatocellular carcinoma *Br. J. Radiol.* **67** 136–9

Leung W T *et al* 1994 Measuring lung shunting in hepatocellular carcinoma with intrahepatic-arterial technetium-99m macroaggregated albumin *J. Nucl. Med.* **35** 70–3

Lewandowski R J and Salem R 2006 Yttrium-90 radioembolization of hepatocellular carcinoma and metastatic disease to the liver *Semin. Intervent. Radiol.* **23** 64–72

Meo S L *et al* 2008 Radiation emission dose from patients administered ^{90}Y-labelled radiopharmaceuticals: comparison of experimental measurements versus Monte Carlo simulation *Nucl. Med. Commun.* **29** 1100–5

Nordion M D S 2004 TheraSphere® Yttrium-90 microspheres (package insert) (Kanata, Canada)

Salem R and Thurston K G 2006 Radioembolization with ^{90}Yttrium microspheres: a state-of-the-art brachytherapy treatment for primary and secondary liver malignancies part 1: technical and methodologic considerations *J. Vasc. Interv. Radiol.* **17** 1251–78

Sanchez-Garcia M, Gardin I, Lebtahi R and Dieudonne A 2014 A new approach for dose calculation in targeted radionuclide therapy (TRT) based on collapsed cone superposition: validation with ^{90}Y *Phys. Med. Biol.* **59** 4769–84

Sarfaraz M, Kennedy A S, Lodge M A, Li X A, Wu X and Yu C X 2004 Radiation absorbed dose distribution in a patient treated with Yttrium-90 microspheres for hepatocellular carcinoma *Med. Phys.* **31** 2449–53

SIRTEX M L 2004 *SIR-Spheres® Yttrium-90 Microspheres (Package Insert)* (Lane Cove: SIRTEX Medical Ltd)

SIRTEX M L 2015 Sirtex medical training manual *Training Program: Physicians and Institutions* (Sydney: SIRTEX Medical Ltd) Available at: http://foxfireglobal.sirtex.com/sites/foxfireglobal.sirtex.com/files/user/trn-rw-04_for_eu_au_nz_and_asia.pdf (Accessed: 5 July 2015)

Snyder W S, Ford M R and Warner G G 1978 *Estimates of Specific Absorbed Fractions for Photon Sources Uniformly Distributed in Various Organs of a Heterogenous Phantom* (New York: Society of Nuclear Medicine) MIRD Pamplet No. 5 (revised)

Tuli J K 1987 *Evaluated Nuclear Structure Data File (ENSDF): a Manual for Preparation of Data Sets* (New York: Brookhaven National Laboratory)

Ziaur R, Shakeel Ur R, Waheed A, Nasir M M, Abdul R and Jahan Z 2012 Absorbed dose estimations of ^{131}I for critical organs using the GEANT4 Monte Carlo simulation code *Chin. Phys.* C **36** 1150